https://doi.org/10.26160/2474-5901-2019-14-45-57

AERODYNAMIC HYSTERESIS FROM THE PERSPECTIVE OF NON-EQUILIBRIUM THERMODYNAMICS

Tsegelskiy V.G., Krylovskiy A.E.

Keywords: hysteresis, hysteresis loop, drag crisis, non-equilibrium thermodynamics.
Abstract. The paper investigates the processes of the airflow around a cylinder and an airplane wing. These aerodynamic processes follow the same evolution laws as the processes in fluid dynamics, heat-mass transfer, magnetism and other physically different systems researched previously. These laws are valid for all the non-equilibrium macroscopic thermodynamic systems, having been confirmed experimentally.

ГИСТЕРЕЗИС В АЭРОДИНАМИКЕ С ПОЗИЦИИ НЕРАВНОВЕСНОЙ ТЕРМОДИНАМИКИ

Цегельский В.Г., Крыловский А.Е.

Ключевые слова: гистерезис, петля гистерезиса, кризис сопротивления, неравновесная термодинамика.
Аннотация. Проанализированы процессы, протекающие при обтекании воздухом цилиндра и крыла самолета. Показано, что с позиции неравновесной термодинамики эти процессы в аэродинамике, так же как исследованные ранее процессы, протекающие в гидрогазодинамике, тепломассообмене, магнетизме и других физически отличающихся системах, подчиняются одним и тем же экспериментально подтвержденным общим закономерностям эволюции неравновесных макроскопических термодинамических систем.

Hysteresis phenomena are well-known in aerodynamics. For example, when measuring the airflow around some airfoils, the lift and drag coefficients obtained experimentally differed when angles of attack α and the Reynolds numbers Re increased and decreased. The angles of attack and Reynolds numbers were determined, at which these coefficients changed rapidly, at times abruptly [1, 2].

In the region of relatively high Re numbers, the drag coefficients of bluff bodies decrease sharply at the specific incident flow velocity corresponding to the critical value of the Reynolds number. For example, at the critical values of Re, the drag coefficient of a sphere decreases almost fourfold.

It was demonstrated that hysteresis occurs in direct and reverse transitions between two quasi-stationary states of a non-equilibrium thermodynamic system in physically different processes [3–5]. These transitions lead to changes in structure (for example, current, boiling, magnetization, etc. depending on the physical process occurring in the system), in thermodynamic characteristics and other parameters. Moreover, structural and parametric changes in the system during transitions occur quite sharply, often intermittently.

Let us consider aerodynamic hysteresis phenomena from the perspective of the non-equilibrium thermodynamics. We will begin by considering the air flow around a cylinder, with a diameter d and a sufficiently large length l. In the region of relatively high Reynolds numbers ($\mathrm{Re} = V_1 \cdot d / \nu$, where V_1 is the incident flow rate, ν is the kinematic viscosity of air) a sharp several-fold decrease in the drag

coefficient of the cylinder is observed. This phenomenon, called the drag crisis, is characteristic of bluff bodies. Fig. 1 shows the experimental drag coefficient C_X as function of Reynolds number.

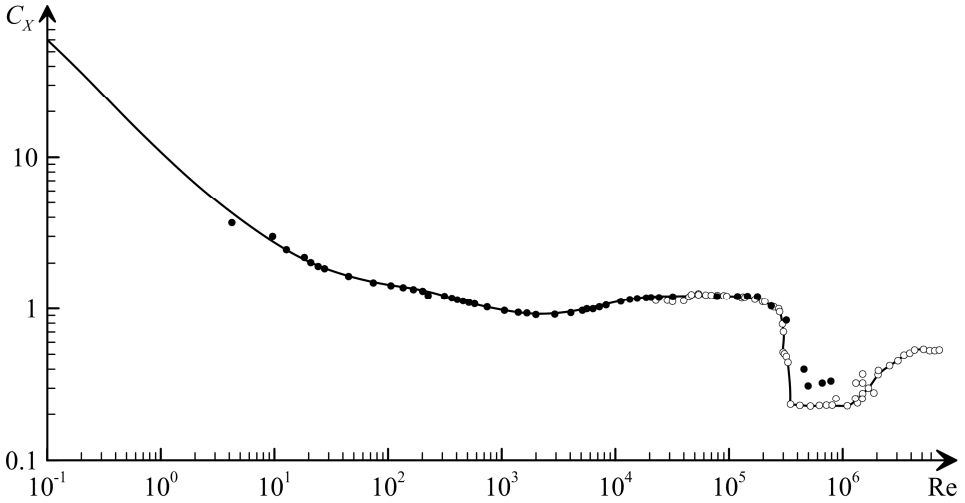

Fig. 1. Drag coefficient of cylinders as function of Re number:
● – Wieselsberger's data [6]; ○ – experiment from [7]

The graph is taken from [6] and is revised for $\mathrm{Re} \geq 2 \cdot 10^4$ according to the subsequent experimental data in [7]. The drag coefficient was determined using the formula $C_X = F_X / \left(0.5 \rho_1 V_1^2 S\right)$, where F_X is drag force, S is the body cross-section relative to the incident flow direction, ρ_1 is the incident flow density. It is evident from Fig. 1 that in the region corresponding to $\mathrm{Re} \approx 2 \cdot 10^4 \ldots 2 \cdot 10^5$, the drag coefficient is practically constant and can be assumed $C_X = 1.22$. This region is often termed "self-similarity" by the Re number. Fig. 2a shows the diagram of the airflow around a cylinder for this range of the Re number values. The gas can be viewed as ideal in its whole volume except for the laminar boundary layer up to its separation line *z*. The tubular vortex area is formed beyond the separation line. In the range of the Reynolds numbers under investigation, the position of the separation line is independent from the Re value. However, as it increases up to $\mathrm{Re} = (2.5 \ldots 3.5) \cdot 10^5$, the drag crisis emerges, which leads to the drag coefficient decreasing almost fivefold. This is determined by the fact that the laminar boundary layer on the body surface becomes unstable and then turbulent. It should be noted that not the entire boundary layer, but only a part of it becomes turbulent. At the beginning of the body surface, the laminar boundary layer is preserved, it is followed by the turbulent boundary layer, and after that the area beyond the separation line. The turbulence transition of the boundary layer leads to a marked displacement of its separation line *z* downstream, as a result, the turbulent vortex trail contracts (see the vortex area in Fig. 2b). The contraction of the vortex trail causes the reduction of drag and, consequently, of the drag coefficient C_X. The drag coefficient decreases abruptly up to $C_X = 0.23$ in a narrow range of the Reynolds numbers and then remains practically stable at up to $\mathrm{Re} \approx 10^6$. This area is the

second “self-similarity” area by Re corresponding to the fixed position of separation line of the turbulent boundary layer.

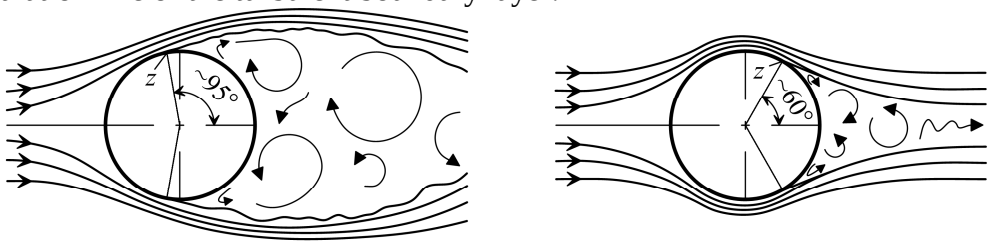

(a) (b)

Fig. 2. Flow patterns around a cylinder: a) in the subcritical range $\mathrm{Re} \approx 2 \cdot 10^4 \ldots 2 \cdot 10^5$; b) in the supercritical region $\mathrm{Re} \approx 3 \cdot 10^5 \ldots 1 \cdot 10^6$

Let us consider a non-equilibrium thermodynamic system as a mass of gas contained in a rectangular block with the height *h* and width *l* between the entry section *1–1* and section *2–2* (Fig. 3). The distance of latter section from the entry equals the distance at which the turbulent trail disappears. Thus we assume that the gas velocity at *2–2* is as uniform across the section as at *1–1*.

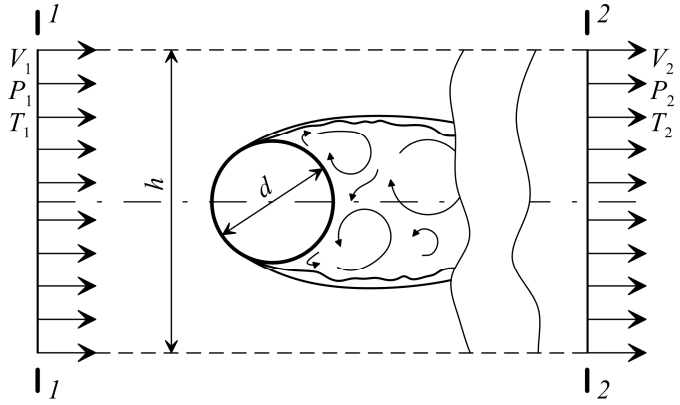

Fig. 3. Section under consideration

Similar to problem 3 in [3] (where laminar and turbulent flow regimes in a cylindrical pipe were analysed in terms of non-equilibrium thermodynamics), let us determine the entropy generation in the thermodynamic system under consideration. We will investigate two quasi-stationary states corresponding to the flow patterns in Fig. 2.

Let us write down the integral equations of mass, momentum and energy conservation for a mass of gas contained in a rectangular block formed by *1–1* and *2–2* sections (Fig. 3):

$$\rho_1 V_1 F = \rho_2 V_2 F = G; \tag{1}$$

$$G V_2 - G V_1 = P_1 F - P_2 F - 0.5 C_X \rho_1 V_1^2 S; \tag{2}$$

$$G\left(C_P T_1 + \frac{V_1^2}{2}\right) = G\left(C_P T_2 + \frac{V_2^2}{2}\right), \tag{3}$$

where P_1, T_1, ρ_1 are the gas pressure, temperature and density at *1–1*; V_2, P_2, T_2, ρ_2 are the gas velocity, pressure, temperature and density at *2–2*; C_P is the gas specific heat capacity at constant pressure; $F = h \cdot l$ is the area of the flow cross-section; G is the flow rate through *1–1* and *2–2*; $S = d \cdot l$ is the area of the cylinder longitudinal section.

In order to estimate only the drag crisis effect on the changes in the thermodynamic parameters of the system, we neglected the shear stress on the side surfaces of the volume. The gas velocity gradients on these surfaces were assumed to approach zero.

We assumed the gas to be ideal, the flow velocity to be subsonic, the pressure, temperature and density to be constant at every point of the entry section *1–1* and the exit section *2–2* (Fig. 3). Then for each section, the equation of state $P / \rho = R_G \cdot T$ is valid, where R_G is the gas constant. For the calculation purposes we assume that the stagnation temperature T_1^* and the total pressure P_1^* at *1–1* remain constant, while the gas flow is adiabatic, which means $T_2^* = T_1^*$, where T_2^* is the stagnation temperature at *2–2*.

From the above equations, we determine the gas flow parameters at *2–2* using the known parameters at *1–1* and the drag coefficient C_X :

$$V_2 = \frac{-b \pm \sqrt{b^2 - 4\,a\,c}}{2a}; \tag{4}$$

$$T_2 = T_1^* - \frac{V_2^2}{2\,C_P}; \tag{5}$$

$$\rho_2 = \frac{\rho_1 V_1}{V_2}; \quad P_2 = \rho_2 R_G T_2, \tag{6}$$

where $a = \frac{1}{2\,C_P} - \frac{1}{R_G}$; $b = \frac{T_1}{V_1} + \frac{V_1}{R_G} - C_X \frac{V_1}{2\,R_G} \cdot \bar{d}$; $c = -T_1^*$; $\bar{d} = \frac{d}{h}$.

Using the given values of T_1^*, P_1^* and $\rho_1^* = \frac{P_1^*}{R_G \cdot T_1^*}$, the gas flow parameters at *1–1* can be conveniently estimated with the help of the following dependences [8]:

$$\frac{P_1}{P_1^*} = \left(1 - \frac{n-1}{n+1}\lambda_1^2\right)^{\frac{n}{n-1}}; \quad \frac{T_1}{T_1^*} = \left(1 - \frac{n-1}{n+1}\lambda_1^2\right); \quad \frac{\rho_1}{\rho_1^*} = \left(1 - \frac{n-1}{n+1}\lambda_1^2\right)^{\frac{1}{n-1}}, \tag{7}$$

where n is adiabatic index, $\lambda_1 = V_1 / a_C$ is the gas superficial velocity at *1–1*; $a_C = \sqrt{\frac{2n}{n+1} R_G \cdot T_1^*}$ is critical velocity.

Let us determine the effect of the Reynolds number on the specific entropy generation *ΠS* in the thermodynamic system under consideration. We will investigate its two possible states corresponding to the gas flow patterns shown in Fig. 2a and 2b. When calculating *ΠS*, gas is viewed as air with the following stagnation parameters in *1–1* cross-section: $P_1^* = 0{,}1$ MPa; $T_1^* = 293$ K and corresponding thermophysical properties, also we assume $\bar{d} = 0{,}05$.

By increasing the superficial air velocity λ_1 at the entry, we determine the flow parameters in section *1–1* and the corresponding Re value by means of formulas (7). We use (4)–(6) to determine the flow parameters in section *2–2* for two values of C_X corresponding to the flow patterns of the cylinder shown in Fig. 2a and 2b. Then we determine the specific entropy generation *ΠS* in the thermodynamic system under consideration for C_X = 1.22 ($ΠS_1$) and C_X = 0.23 ($ΠS_2$) using the known equation given, for example, in [3]:

$$ΠS = C_P \ln \frac{T_2}{T_1} - R_G \ln \frac{P_2}{P_1}.$$

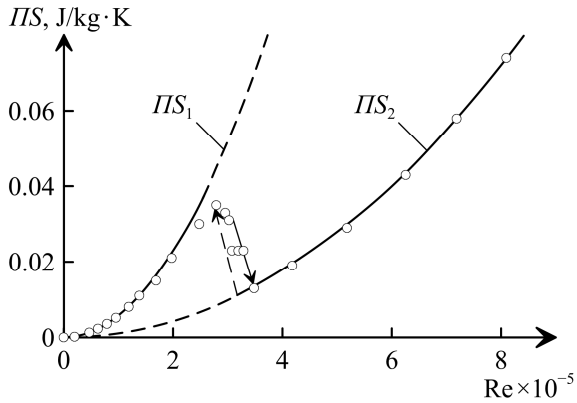

Fig. 4. Specific entropy generation as function of Re number for the flow around a cylinder ($ΠS_1$: flow pattern for Fig. 2a; $ΠS_2$: flow pattern for Fig. 2b)

The specific entropy generation production *ΠS* is the amount of entropy that occurs within the system per unit of time in relation to the gas flow rate. Fig. 4 shows the calculated dependences of the specific entropy generations $ΠS_1$ и $ΠS_2$ on the Reynolds number as lines, and the similar dependences constructed with a number of experimental C_X values as dots [7]. It is evident from the graph that the increase in the Reynolds number leads to such critical values that the non-equilibrium thermodynamic system changes from a higher to lower entropy quasi-stationary state. The decrease in the Re number results in the reverse transition: from a lower entropy state $ΠS_2$ (corresponds to the structure of a flow over a cylinder in Fig. 2b) to a higher entropy state $ΠS_1$ (structure in Fig. 2a).

According to the axiom concerning all natural processes seeking perfection formulated in [9] and experimentally confirmed for various physical processes in nature [3–5, 10]):

In a thermodynamic system, of the all possible stationary states within the nature laws, irreversible thermodynamics, boundary and other physical conditions, that state is the most likely which involves the minimally possible entropy generation.

The minimal-entropy state $ΠS_2$ can be realized due to the existence of a stable turbulent boundary layer on the surface of a cylinder.

According to the general laws of the changes in the states of non-equilibrium thermodynamic systems [3, 4], the transition of a non-equilibrium thermodynamic

system from a higher to lower entropy stationary state occurs when, in the process of the system's evolution, the difference between the entropy generations of these two states reaches a certain positive value. This statement is in full compliance with the dependences in Fig. 4.

In the case under consideration, the higher to lower entropy transition is determined by the loss of stability of the laminar boundary layer that is formed on the cylinder at the initial moment due to the internal or external disturbances to the flow.

Thus, the drag crisis phenomenon in bluff bodies is a transition of a non-equilibrium thermodynamic system from a higher entropy quasi-stationary state (flow structure as in Fig. 2a) to a lower entropy quasi-stationary state (flow structure as in Fig. 2b).

According to the general laws [3, 4], transitions (direct and reverse) between the states of a non-equilibrium thermodynamic system must exhibit hysteresis, with thermodynamic parameters and flow patterns changing sharply, even abruptly during these transitions. However, in the fundamental works (for example [6]) and many others, which are concerned with the drag crisis of bluff bodies, hysteresis is not mentioned. It involved great effort to find a paper [7] experimentally confirming hysteresis in the direct and reverse transitions between the two states of a non-equilibrium thermodynamic system.

Fig. 5 shows the drag force F_X of a cylinder as function of Reynolds number in the near-critical region [7]. When the Reynolds number increases, the direct transition from the state corresponding to the flow pattern in Fig. 2a to the state corresponding to the flow pattern in Fig. 2b, is accompanied by two abrupt changes (*A* and *B)* in the force F_X (Fig. 5). During the transition *A*, the laminar boundary layer is turbulized on the wall on one side of the cylinder, which leads to an asymmetric flow in a narrow range of Re numbers. The transition *B* from an asymmetric to a symmetric flow (Fig. 2b) occurs at somewhat higher Re values due to the turbulization of the laminar boundary layer on the other side of the cylinder. Transitions B' and A' in Fig. 5 correspond to the reverse transition at the decrease in the Reynolds number. It can be evident that the direct and reverse transitions are realized through hysteresis. In Fig. 4 arrows indicate the Re values (corresponding to the experimental curve in Fig. 5) when the transition from one flow pattern around a cylinder to another occurs, for example, from subcritical (Fig. 2a) to supercritical (Fig. 2b) flow pattern and in reverse.

Thus, the transitions from higher to lower entropy state and back in the non-equilibrium thermodynamic system under consideration are characterized by abruptness and accompanied by hysteresis as in other non-equilibrium thermodynamic systems [3–5, 10].

However, a relatively stable asymmetric flow emerges in the process of transition from one quasi-stationary state to another in the narrow range of Re numbers. This flow turns into an absolutely stable symmetric flow only when there is strong perturbation. This is similar to Rayleigh-Benard convection, when a stable three-dimensional flow with a characteristic asymmetry between the upper and lower half of the layer may occur during the unstable flow development [11].

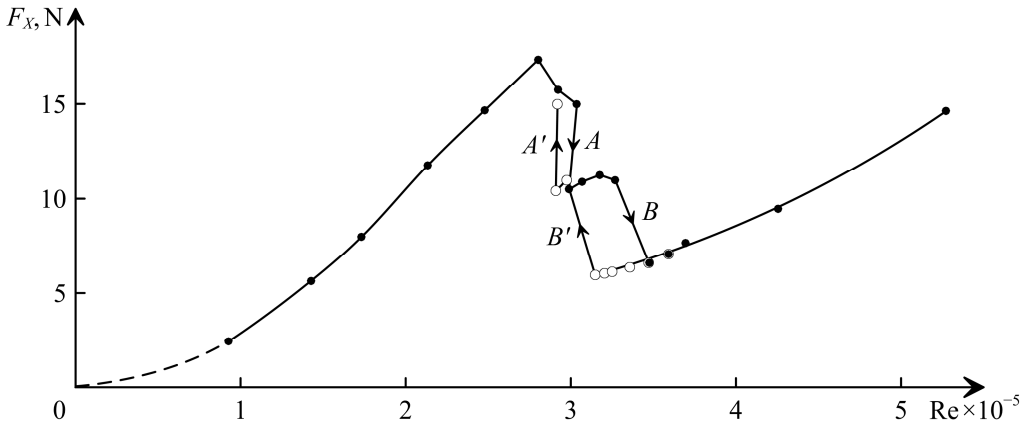

Fig. 5. Hysteresis effects of *A* and *B* transitions (Re increasing); *B′* and *A′* (Re decreasing)

Let us now consider the airflow around small wings in the range $\mathrm{Re} = 4 \cdot 10^4 \ldots 2 \cdot 10^5$. In this case, the reference length for determining the Reynolds number is the chord airfoil length. The flow pattern around small wings is similar to the flow pattern around a cylinder considered above. Fig. 6 shows the drag coefficient C_X and the lift coefficient C_Y of the wing as function of Re. The presented curves were obtained for the flow around the airfoil N 60 at an angle of attack of 10° [1]. Similar curves were obtained for other angles of attack and airfoils.

At low Reynolds numbers, a laminar boundary layer is formed on the upper front surface of the airfoil. This layer separates at point *z*, since it cannot overcome the pressure increase somewhat earlier (Fig. 6a, left). This flow pattern corresponds to the *AFB* sectors of the drag and lift coefficient experimental curves in Fig. 6b, 6c.

As the Reynolds number increases, it reaches the critical value, at which the laminar boundary layer becomes turbulent, and the separation point *z* moves downstream (see Fig. 6a, right). At the same time, the area of the vortex trail sharply decreases, and, as a result, the drag coefficient C_X decreases intermittently. At the same time, the lift coefficient increases abruptly. This transition corresponds to the *BC* sections in Fig. 2b and 2c represented by dotted lines with the direction of the transition indicated by an arrow. With a further increase in Re, the flow pattern around the wing is basically preserved, which corresponds to *CD* in the experimental curves. When the velocity decreases, the reverse transition occurs at the Reynolds number significantly lower than the critical values of the direct transition. The reverse transition is represented by arrows *EF* in Fig. 6b, 6c.

It should be noted that the critical Reynolds number depends on the angle of attack, the shape and profile of the wing, the degree of turbulence of the incident flow and other factors. The comparison of Fig. 6b and Fig. 6c demonstrate that a sharp decrease in the drag coefficient C_X leads to the equally sharp increase in the lift coefficient C_Y, and vice versa: an increase in C_X leads to a decrease in C_Y.

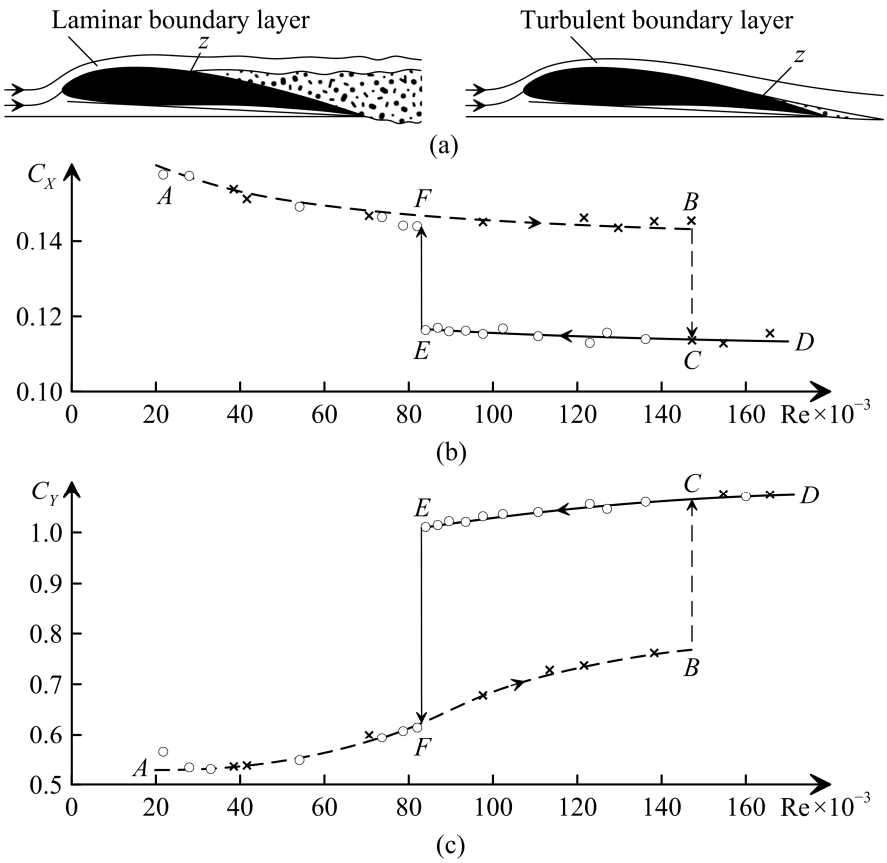

Fig. 6. Flow patterns corresponding to two quasi-stationary states (a); drag coefficient C_X as function of Re (b); lift coefficient C_Y as function of Re (c) [1]

Fig. 7 shows the specific entropy generation as a function of Re. These dependences are constructed for the *AFB* (ΠS_1) and *ECD* (ΠS_2) sections of the experimental curves in Fig. 6b. The specific entropy generation for the two airfoil flow patterns in Fig. 6a was calculated in a similar way as for that of a cylinder. It follows that in the non-equilibrium thermodynamic system under consideration, and in the system analysed above, transitions from one quasi-stationary state to another one and back are realized through hysteresis. These transitions are accompanied by abrupt changes in both the parameters and the structure (flow pattern) of the thermodynamic system. As is the case with a cylinder, the higher to lower entropy transition of a quasi-stationary non-equilibrium thermodynamic system occurs when there is a certain positive difference between the entropy generation of these states. The lower to higher entropy state transition of the same thermodynamic occurs when the conditions are reached when a stable turbulent boundary layer on the wing surface becomes impossible. Therefore, turbulization of the boundary layer on the wing tip will help delay the lower to higher entropy transition of the thermodynamic system. This is confirmed by numerous experiments, for example, with a tripwire at the beginning of the wing or the appropriate change in the shape of the leading edge.

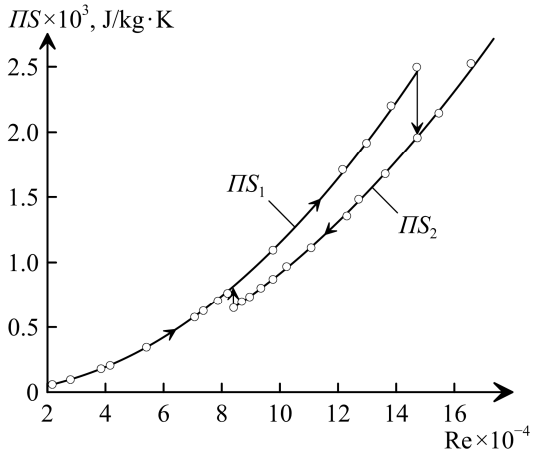

Fig. 7. Specific entropy generation as function of Re for the flow around a wing (ΠS_1 for the flow pattern in Fig. 6a, left; ΠS_2 for the flow pattern in Fig. 6a, right)

Nature also seeks perfection in creating certain conditions. For example, bird's wing, as well as some insects' wings, have the profile and high relative roughness suited for flying with a turbulized boundary layer. A dragonfly's wing is equipped with transverse folds and sharp-toothed front edges for turbulization of the boundary layer.

The hysteresis in the aerodynamic forces also manifests itself through the changes in the angles of attack during the subsonic flow, which is confirmed by numerous experimental studies. For example, Fig. 8 shows the aerodynamic coefficient C_Y as function of the angle of attack [12]. The curves are plotted for a rectangular wing (profile NACA 0018) for two fixed flow rates: 20 m/s and 35 m/s. During the experiment, the angle of attack changed quasi-stationary, first upward (forward), and then downward (reverse). In both cases, the dependences have the form of hysteresis loops. According to [3–5, 9], hysteresis occurs in the parametric range within which at least two quasi-stationary, structurally different states can exist in the non-equilibrium thermodynamic system under consideration.

In the section $C_Y = f(\alpha)$ (corresponding to the upper branch of the hysteresis loop in Fig. 8a), the flow on the wing upper surface at small angles of attack is practically separation-free. However, as α increases and approaches the critical angle of attack, in the trailing edge of the wing there emerge small symmetric separation flow regions. The emergence of these regions changes the linear nature of the dependence $C_Y = f(\alpha)$. At critical α value, C_Y decreases sharply.

In the section $C_Y = f(\alpha)$ (corresponding to the lower branch of the hysteresis loop), the flow separates completely along the entire leading edge of the wing at large angles of attack, and the so-called stagnant zone is formed. With a further decrease in the angle of attack, the separation of the flow around the wing remains, but small, symmetric regions of separation-free flow emerge on a part of its leading edge. This results in an increase in C_Y on the lower branch of $C_Y = f(\alpha)$ (Fig. 8a). A further decrease in the angle of attack leads to a sharp increase in C_Y and a change in the flow pattern around the wing, which becomes separation-free.

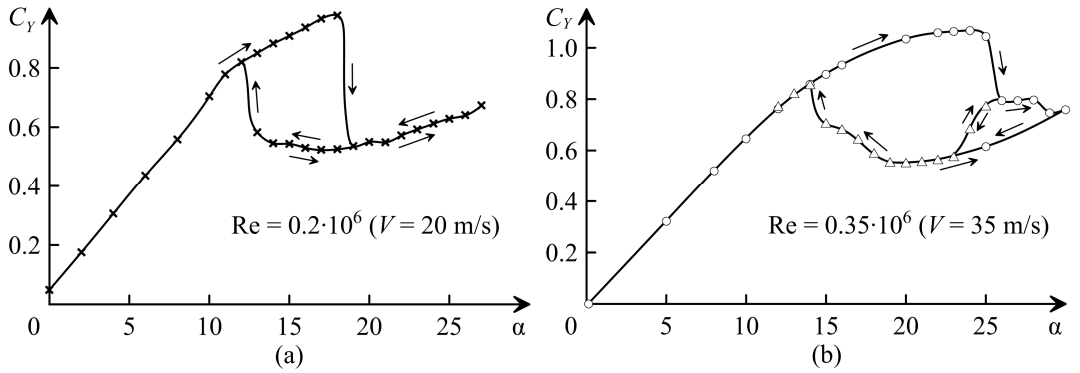

Fig. 8. Aerodynamic coefficient C_Y as function of angle of attack:
a) Re = $2 \cdot 10^6$; b) Re = $0.35 \cdot 10^6$

Data from experiments (for example, [2, 12]) indicate the curves of C_Y and C_X as functions of α are smooth in those intervals of angles of attack where the flow changes in an evolutionary way and there is no fundamental transformation. These coefficients change abruptly only with the alteration of the flow pattern.

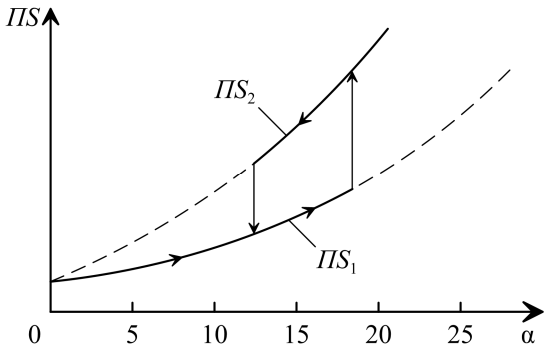

Fig. 9. Change in the specific entropy generation as function of angle of attack:
ΠS_1 – separation-free flow regime; ΠS_2 – complete separation flow regime

Fig. 9 shows the character of the specific entropy generation as a function of angle of attack. ΠS_1 corresponds to a separation-free flow around the wing, and ΠS_2 corresponds to a complete separation. The arrows indicate the directions of transitions from one flow pattern to another. This case, as the other cases considered above, complies with the general laws of the non-equilibrium thermodynamic system evolution [3, 4]. In particular, the non-equilibrium thermodynamic system transits from the lower to higher entropy generation state (ΠS_1 to ΠS_2) because a physical condition is not fulfilled, i.e. the boundary layer on the wing surface loses its stability. This transition is quite abrupt, with highly unsteady, unstable flow patterns. When the critical angle of attack is exceeded, there is a separation of the flow from the leading edge in different parts of the wing. As α continues to increase, these separation zones connected to the diffuser separation region. The number, size and location of the separation regions vary randomly both in time and along the wing surface, until at some value of α a new

quasi-stationary flow pattern emerges, characterized by an almost complete separation of the flow on the wing.

This process of transition from one quasi-stationary flow pattern to another in a non-equilibrium thermodynamic system is similar to the process of transition from laminar to turbulent flow regime in a pipe [3] or from nucleate to film boiling regimes [4]. The laminar to turbulent flow regime transition also occurs through unsteady states in a certain narrow range of Re numbers. The turbulized and laminar gas flow regions continuously alternate both in time and space. When a nucleate boiling regime transits to a film boiling regime, various combinations of these two regimes form and erratically replace each other in different areas of the heat-transfer surface.

Comparison of the hysteresis loops in Fig. 8a and 8b demonstrates that in the latter case, in the transition from the separation-free flow to the complete separation flow, a certain intermediate flow pattern emerges in a narrow range of angles of attack. Visualization of the flow pattern [12] corresponding to this intermediate structure showed that the flow around the wing in this case is essentially asymmetric and independent from the direction of the angular displacement. This is similar to the formation of an asymmetric flow pattern around a cylinder in transition from one branch of the hysteresis loop to another (Fig. 5).

In aerodynamics, both the clockwise and counter-clockwise hysteresis is possible, depending on the varied parameter (argument) in the experiment and the corresponding selected function. Fig. 4, 5, 6b, 7 and 8 present clockwise hysteresis, while Fig. 6c and 9 present counter-clockwise hysteresis. The direction of hysteresis can be influenced by a number of factors including the airfoil.

It can be concluded that from the perspective of non-equilibrium thermodynamics, the aerodynamic processes described above are similar to those in fluid dynamics, heat and mass transfer, magnetism, etc. [3–5, 9].

These processes occur in physically different non-equilibrium thermodynamic systems. However, they comply with the same experimentally confirmed general laws (rules) governing the changes in the state of such systems [3, 4].

References

1. Schmitz, F.W. Aerodynamics of the Model Airplane. Part I. Airfoil Measurements (Translated from German). RSIC – 721. 22 November 1967. 201 p.
2. Ryzhov Yu.A., Stolyarov G.I., Tabachnikov V.G. Critical regimes of the transformation of a flow pattern around a rectangular wing under subsonic unsteady flow // Scientific notes of TSAGI. 1996. Vol. XXVII. Issue 3-4. P. 3-12.
3. Tsegelskiy V.G. On application of non-equilibrium thermodynamics for solving of hydrodynamic problems and definition of human activity influence on Earth climate // Journal of Advanced Research in Technical Science. 2017. Issue 6. P. 23-47.

4. Tsegelskiy V.G. Thermodynamic analysis of the impact of world energy and other aspects of human activity on the approach of the ice age on Earth // Journal of Advanced Research in Technical Science. 2018. Issue 9-1. P. 5-20.
5. Tsegelskiy V.G. Hysteresis in magnetics from a position of non-equilibrium thermodynamics // Journal of Advanced Research in Technical Science. 2018. Issue 10 1. P. 28-38.
6. Schlichting H. Boundary-layer Theory. Moscow: Science, 1974. 712 p.
7. Günter Schewe. On the force fluctuations acting on a circular cylinder in crossflow from subcritical up to transcritical Reynolds numbers // J. Fluid Mech. 1983. Vol. 133. P. 265-285.
8. Abramovich G.N. Applied Gas Dynamics. Moscow, Nauka Publ., 1976. 888 p.
9. Tsegelskiy V.G. On the application of irreversible thermodynamics processes for the calculation of the supersonic ejector operating modes // Proceedings of the universities, Mechanical engineering, 2015. No 6. P. 26-45.
10. Tsegelskiy V.G. Jet devices. M.: MSTU named. N.E. Bauman, 2017. 576 p.
11. Getling A.V. Rayleigh-Benard Convection. Moscow, Editorial URSS Publ., 1999. 248 p.
12. Kabin S.V., Kolin V.I., Svyatodukh V.K., Sukhanov B.L., Shukhovtsov D.V. Multiple hysteresis of static aerodynamic characteristics // Scientific notes of TSAGI. 1999. Vol. XXX. Issue 3-4. P. 61-68.

Список литературы

1. Schmitz, F.W. Aerodynamics of the Model Airplane. Part I. Airfoil Measurements (Translated from German). RSIC – 721. 22 November 1967. 201p.
2. Рыжов Ю.А., Столяров Г.И., Табачников В.Г. Критические режимы перестройки структуры обтекания прямоугольного крыла при дозвуковом нестационарном обтекании // Ученые записки ЦАГИ. 1996. Том XXVII. № 3-4. С. 3-12.
3. Цегельский В.Г. О применении неравновесной термодинамики в решении гидродинамических задач и в определении воздействия жизнедеятельности человека на климат Земли // Journal of Advanced Research in Technical Science. 2017. Issue 6. P. 23-47.
4. Tsegelskiy V.G. Thermodynamic analysis of the impact of world energy and other aspects of human activity on the approach of the ice age on Earth // Journal of Advanced Research in Technical Science. 2018. Issue 9-1. P. 5-20.
5. Цегельский В.Г. Гистерезис в магнетизме с позиции неравновесной термодинамики // Journal of Advanced Research in Technical Science. 2018. Issue 10-1. P. 28-38.
6. Шлихтинг Г. Теория пограничного слоя. М.: Наука, 1974. 712 с.
7. Günter Schewe. On the force fluctuations acting on a circular cylinder in crossflow from subcritical up to transcritical Reynolds numbers // J. Fluid Mech. 1983. Vol. 133. P. 265-285.

8. Абрамович Г.Н. Прикладная газовая динамика. М.: Наука, 1976. 888 с.
9. Цегельский В.Г. О применении термодинамики необратимых процессов в расчетах режимов работы сверхзвукового эжектора // Изв. вузов, Машиностроение. 2015. № 6. С. 26-45.
10. Цегельский В.Г. Струйные аппараты. М.: МГТУ им. Н.Э. Баумана, 2017. 576 с.
11. Гетлинг А.В. Конвекция Рэлея-Бенара. М.: Эдиториал УРСС, 1999. 248 с.
12. Кабин С.В., Колин В.И., Святодух В.К., Суханов В.Л., Шуховцов Д.В. Множественный гистерезис статических аэродинамических характеристик // Ученые записки ЦАГИ. 1999. Том. XXX, № 3-4. С. 61-68.

Цегельский Валерий Григорьевич – доктор технических наук, главный научный сотрудник Московского государственного технического университета им. Н.Э. Баумана, г. Москва, РФ	**Tsegelskiy Valery Grigorievich** – Doctor habilitatus, Chief Scientist of Bauman Moscow State Technical University, Moscow, Russian Federation
Крыловский Александр Евгеньевич – инженер ООО «Техновакуум», г. Москва, РФ	**Krylovskiy Alexsandr Eugenievich** – engineer of «Technovacuum» Ltd, Moscow, Russian Federation

Received 19.02.2019